EPJ Web of Conferences **97**, 00005 (2015)
DOI: 10.1051/epjconf/ 20159700005

Hyperon Production in pp Collisions at $\sqrt{s} = 7$ TeV at the LHC with ALICE

Alexander Borissov[1,a] for the ALICE Collaboration

[1] *Pusan National University, Pusan, South Korea*

Abstract. The $\Sigma^0(\bar{\Sigma}^0)$ baryon is studied in the transverse momentum range between 1 and 10 GeV/c using the unique capability of the ALICE detector to measure low energy photons. The production of the strange and double-strange baryon resonances $(\Sigma(1385)^{\pm}, \Xi(1530)^0)$ has been measured at mid-rapidity ($|y| < 0.5$) in proton-proton collisions at $\sqrt{s} = 7$ TeV. Transverse momentum spectra are compared to QCD-inspired models, which in general underpredict the data.

1 Introduction

The study of strange baryons and their resonances in proton-proton (pp) collisions contributes to the understanding of hadron production mechanisms and provides a reference for tuning QCD-inspired event generators [1]. The strange-quark content makes these baryons a valuable tool in understanding production mechanisms, since the initial colliding projectiles contain no strange valence quarks and therefore all strange particles are created in the collision.

In addition, a measurement of resonance production in the pp system serves as a reference for understanding resonance production in heavy-ion collisions. Many resonances have lifetimes of a few fm/c, comparable to the lifetime of the hadronic phase [1, 2] and are sensitive probes of the dynamical evolution of the fireball. Previous measurements at a collision energy $\sqrt{s} = 0.2$ TeV with the STAR detector at RHIC have shown that the yields of $\Sigma(1385)^{\pm}$ in Au–Au in comparison to pp collisions indicate the presence of rescattering and regeneration in the time span between chemical and kinetic freezeout [2]. A forthcoming analysis of strange baryon resonances in Pb–Pb collisions by the ALICE collaboration will further explore those effects at higher energy and density of the colliding system. The published ALICE results in pp collisions [1] will therefore serve as benchmark for the $\Sigma(1385)^{\pm}$ and $\Xi(1530)^0$ baryons [1].

While yields of Σ^0 have been measured in many different colliding systems at low and intermediate/moderate energies, only one measurement exists in high energy nuclear collisions. The STAR detector reconstructed the electromagnetic $\Sigma^0 \rightarrow \Lambda+\gamma$ decay via the weak decay of the $\Lambda \rightarrow p+\pi^-$ and γ conversions into e^+e pairs in the detector material [3]. There, the cross section ratio $\Sigma^0/\Lambda = 0.16^{+0.41}_{-0.09}$ was measured in minimum bias 0.2 TeV d+Au collisions. High energy nuclear collisions are of particular interest due to the possibility of measuring isospin degeneracy factors from Σ^0 and Λ yields and of opening new channels of hyperon production via partonic degrees of freedom [4].

[a] e-mail: Alexander.Borissov@cern.ch
[1] Antiparticles here and below are not listed for brevity.

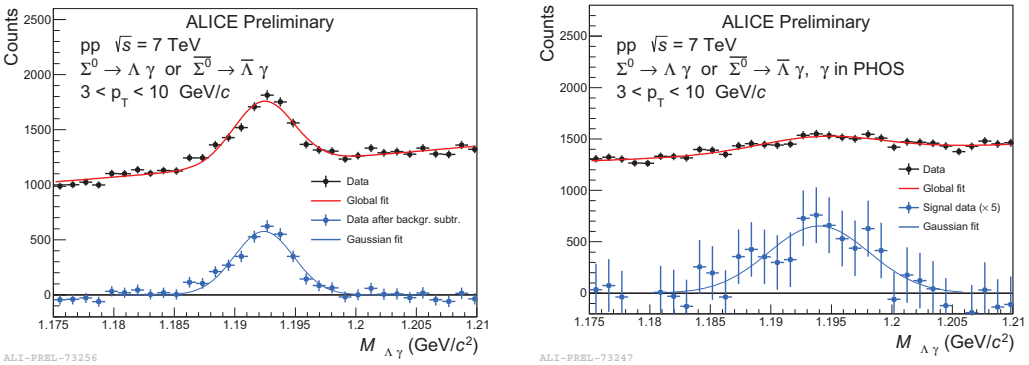

Figure 1. Invariant mass of $\Lambda\gamma$ and $\bar{\Lambda}\gamma$ pairs, where the Λ or $\bar{\Lambda}$ is detected in the central tracking system and the photon is detected using the conversion method (left) or PHOS (right). The red curves are fits to the data using Gaussian peaks plus fourth-order polynomials to describe the background. The invariant mass distribution after the background subtraction is presented on the bottom part of the plot.

2 Detection of Σ^0 Hyperon

The data analysis is carried out using a sample of ~250 million minimum-bias pp collisions at $\sqrt{s}$ = 7 TeV collected during 2010 run at the LHC.

The Σ^0 is reconstructed through the decay $\Sigma^0 \rightarrow \Lambda + \gamma$. The Λ is identified through its decay to a proton and a π^-, while the photon is detected through its conversion to an e^+e^- pair. Tracks from the secondary vertex (V0) are reconstructed in the ALICE tracking system, which consists of the Inner Tracking System (ITS) and the Time Projection Chamber (TPC) [5]. The combined acceptance of the ITS and TPC is $|\eta| < 0.9$. The pairs of tracks are selected using a secondary vertex finding algorithm which is described in detail in Refs. [1, 5, 6].

Further refinment of the sample of converted photons and rejection of weak decays, mainly from K^0_s and Λ, is performed using electron identification via dE/dx and the restriction of the opening angle between electron and positron. This method of reconstruction is called the photon conversion method (PCM). The probability of photon conversion in the central tracking system is ~ 0.08 and the reconstruction efficiency is about 0.67 [7]. To reduce the combinatorial background, a restriction on the Σ^0 phase space (an Armenteros-Podolanski cut) was used: $\alpha = |\frac{p_l^\gamma - p_l^\Lambda}{p_l^\gamma + p_l^\Lambda}| > 0.6$ and $p_t < 0.1$, where p_l^i is the longitudinal momentum of a particle i (γ or Λ) with respect to the Σ^0 momentum direction, and p_t corresponds to transverse momentum of Λ with respect to the Σ^0 momentum. A clean Σ^0 invariant mass peak reconstructed using this technique is presented in the left panel of Fig. 1.

The electromagnetic calorimeter PHOS, see Ref. [5], is made of $PbWO_4$ crystals and has fine granularity with crystal size $2.2 \times 2.2 \times 18$ cm^3. It is located 4.6 m from the interaction point. PHOS subtends $260^o < \phi < 320^o$ in azimuth and $|\eta| < 0.13$ in pseudorapidity. Its energy resolution is $\Delta E \sim 3\%/\sqrt{E_\gamma(\mathrm{GeV})} \oplus 1.1\%$. Data from PHOS were used for Σ^0 detection as a proof-of-principle, see right panel of Fig. 1.

The combined $\Sigma^0 + \bar{\Sigma}^0$ signals are presented in Fig. 1 for the two independent photon detection methods: photon-conversion method (left) and photon detection in PHOS (right). The peaks are fitted using a Gaussian peak added to a polynomial that describes the background. These fits have χ^2/ndf approximately equal to 1.

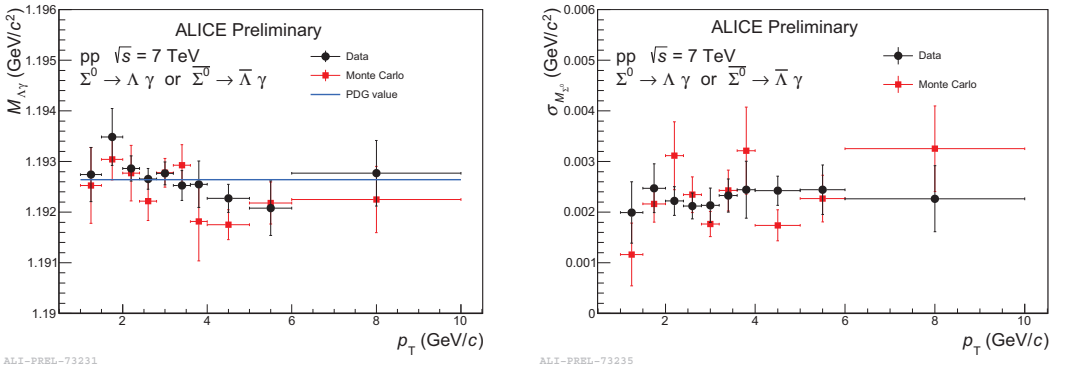

Figure 2. Mean value (left panel) and width (right panel) of the extracted Σ^0 and $\bar{\Sigma}^0$ invariant mass as functions of p_{T} bins from 2010 data (black circles) and simulated events (red squares).

Table 1. Parameters extracted from the Levy-Tsallis fits to the transverse momentum spectra [1]. The values of $\mathrm{d}N/\mathrm{d}y$ are calculated using the spectra in the measured range and the extrapolation of the fitted Levy-Tsallis function outside the measured range. First the statistical and second the systematic uncertainties are quoted here. Systematic uncertainties are the ones derived from the Levy-Tsallis fits only.

Baryon	$\mathrm{d}N/\mathrm{d}y(\times 10^{-3})$	C(MeV)	n	$\langle p_{\mathrm{T}} \rangle$ (GeV/c)
$\Sigma(1385)^+$	$9.8 \pm 0.2 \pm 0.9$	$301 \pm 39 \pm 15$	$9.0 \pm 2.9 \pm 0.5$	$1.17 \pm 0.02 \pm 0.03$
$\Sigma(1385)^-$	$10.6 \pm 0.2 \pm 1.1$	$308 \pm 39 \pm 20$	$9.1 \pm 3.2 \pm 0.8$	$1.17 \pm 0.02 \pm 0.03$
$\bar{\Sigma}(1385)^-$	$9.0 \pm 0.2 \pm 0.9$	$307 \pm 40 \pm 15$	$9.8 \pm 3.7 \pm 0.8$	$1.18 \pm 0.02 \pm 0.04$
$\bar{\Sigma}(1385)^+$	$10.0 \pm 0.2 \pm 1.1$	$294 \pm 43 \pm 17$	$8.9 \pm 3.5 \pm 0.6$	$1.18 \pm 0.02 \pm 0.04$
$\Xi(1530)^0$	$2.48 \pm 0.07 \pm 0.24$	$404 \pm 20 \pm 21$	$16.9 \pm 3.9 \pm 1.9$	$1.33 \pm 0.02 \pm 0.05$

The good energy resolution of the PCM [5, 7] allows Σ^0 invariant mass peak to be reconstructed in the p_{T} region from 1 up to 10 GeV/c, see the left panel on Fig. 2. There is good agreement between the mean value of the Σ^0 mass and the vacuum value presented as a solid line.

The reconstructed width of the Σ^0 is around 2.5 MeV and its value is in agreement with the value from simulations, see Fig. 2 right panel. These results allow the continuation of the Σ^0 analysis towards the extraction of its p_{T} spectra and an evaluation of $\Sigma^0/\Lambda(p_{\mathrm{T}})$ cross section ratio from pp collisions at $\sqrt{s} = 7$ TeV, as well as the analysis of ALICE data from proton-Pb and Pb-Pb collisions.

3 p_{T} spectra of $\Sigma(1385)^{\pm}$ and $\Xi(1530)^0$

The analysis of $\Sigma(1385)^{\pm}$ and $\Xi(1530)^0$ hyperons is described in detail in [1]. Therefore, we present only a selection of results from $\Sigma(1385)^{\pm}$ and $\Xi(1530)^0$ p_{T} spectra analysis are presented below.

The spectra of $\Sigma(1385)^{\pm}$, $\bar{\Sigma}(1385)^{\pm}$ and $\Xi(1530)^0$ are fitted with a Levy-Tsallis function [8]: $\frac{1}{N_{INEL}} \frac{\mathrm{d}^2N}{\mathrm{d}y\mathrm{d}p_{\mathrm{T}}} = \frac{(n-1)(n-2)}{nC[nC+m_0(n-2)]} \frac{\mathrm{dN}}{\mathrm{dy}} p_{\mathrm{T}} (1 + \frac{m_{\mathrm{T}}-m_0}{nC})^{-n}$, where $m_{\mathrm{T}} = \sqrt{m_0^2 + p_{\mathrm{T}}^2}$. Table 1 presents the results of the fit, together with the mean transverse momentum $\langle p_{\mathrm{T}} \rangle$. The anti-baryon to baryon ratios of $\bar{\Sigma}(1385)^-/\Sigma(1385)^+$ and $\bar{\Sigma}(1385)^+/\Sigma(1385)^-$ as functions of p_{T} are compatible with unity [1].

The transverse momentum spectra of both $\Sigma(1385)^{\pm}$ are compared to standard tunes of PYTHIA 6 [9], PYTHIA 8 [10], HERWIG [11] and SHERPA [12] in Fig. 3. For all applied generators the overall

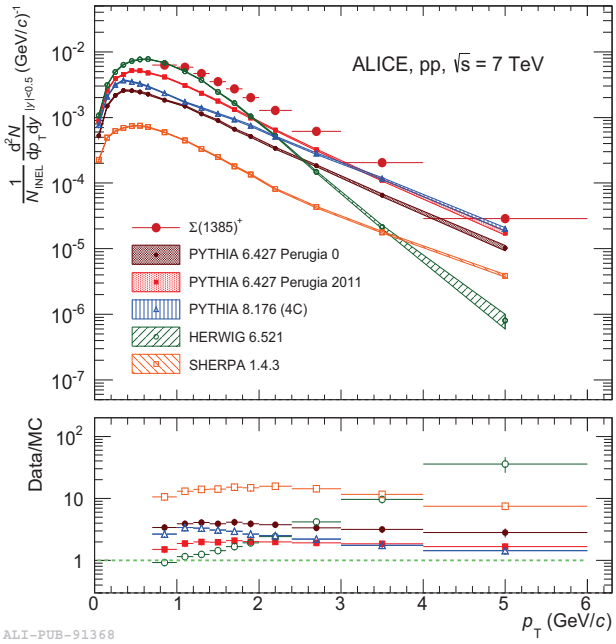

Figure 3. The transverse momentum spectrum of $\Sigma(1385)^+$ is compared to standard tunes of PYTHIA 6 [9] and PYTHIA 8 [10], the latest release of HERWIG (6.521) [11], and SHERPA release 1.4.6 [12]. The MC data are binned according to the data. Spectra points are plotted at the center of the p_{T} interval. The lower panel shows the ratio data/MC. p_{T}-independent uncertainties are not shown.

production cross sections are largerly underestimated. The same is true for the $\Xi(1530)^0$ when its p_{T} spectrum is compared to the same set of generators [1]. Note, that upcoming ALICE data will allow more detailed investigation of the hyperon production at LHC, including its study in the underlying soft events and within jets.

References

[1] ALICE Collaboration, [nucl-ex/ 1406.3206], accepted in Eur. Phys. J. C
[2] STAR collaboration, Phys. Rev. Lett. **97** (2006) 132301, [nucl-ex/0604019]
[3] G. Van Buren for the STAR Collaboration, [nucl-ex/0512018];
G. Van Buren for the STAR Collaboration, J.Phys. G **31**, 195 (2005)
[4] P. Koch and J. Rafelski, Nucl. Phys. A **444**, 678 (1985)
[5] ALICE Collaboration, Int. J. Mod. Phys. A **29**, 1430044 (2014)
[6] ALICE Collaboration, Eur. Phys. J. C **71**, 1594 (2011)
[7] ALICE Collaboration, Phys. Lett. B **717**, 162-172 (2012)
[8] C. Tsallis, J. Stat. Phys. **52**, 479 (1988)
[9] T. Sjostrand, S. Mrenna, and P. Skands, J. High Energy Phys. **05**, 026 (2006)
[10] T. Sjostrand, S. Mrenna, and P. Skands, Comput. Phys. Comm. **178** 852 (2008)
[11] G. Corcella, I. Knowles, G. Marchesini et al, J. High Energy Phys. **0101** 010 (2001)
[12] T. Gleisberg, S. Hoche, F. Krauss et al, J. High Energy Phys. **02** 007 (2009)